This article has been accepted for publication in IEEE Antennas and Wireless Propagation Letters. This is the author's version which has not been fully edited and content may change prior to final publication. Citation information: DOI 10.1109/LAWP.2024.3371930

Fast Design of Ultra-Wideband Absorbers Based on Equivalent Circuit Model

Xianglin Kong, *Member, IEEE*, Shengjun Zhang, Xiaoyu Pang, Yixiang Fu, Lei Zhao, *Senior Member, IEEE*, Zhongxiang Shen, *Fellow, IEEE*

***Abstract*—A fast method is presented for designing ultra-wideband absorbers composed of resistive surfaces (RSs), substrates and metallic plate. A general effective permittivity for RSs printed on stratified dielectrics under considering metallic plate is derived to obtain the closed-form relationships between resistance, capacitance and absorber parameters. An equivalent circuit (EC) is developed for absorbers to combine with genetic algorithm to quickly achieve an optimal value of lumped elements, thereby calculating absorber parameters. Utilizing the proposed approach, an absorber within 0.64-41.7 GHz with reflection loss lower than -10 dB is obtained efficiently. The close match between the EC model and full-wave simulation results shows accuracy of the proposed approach. To further verify the proposed method, a 1.16-19.2 GHz absorber was designed and manufactured, and the measurements agreed well with the EC and full-wave simulations.**

***Index Terms*—Ultra-wideband absorber; resistive surfaces; equivalent circuit model.**

I. INTRODUCTION

Broadband absorbers have the ability to dissipate the electromagnetic waves energy across a wide frequency range. The most commonly used methods for designing wideband absorbers are multi-layered stacking or planar arrangement of lossy surfaces [1-3], loading resistive surfaces (RSs) [4-8], and lumped resistive elements [9-12]. RSs have been widely used to design wideband absorbers due to its good ohmic loss [13-18]. However, wideband absorbers design is complicated due to many factors referring to absorption characteristics. Therefore, it is essential to develop simple way for their design.

To facilitate the design of absorbers, it is crucial to establish closed-form expressions between resistance, inductance, capacitance in EC model and geometric parameters of the resistive surface [19-25]. However, the accuracy of these expressions relies on the effective permittivity, which is influenced by factors such as the number, thickness, and permittivity of the surrounding dielectrics. While an effective permittivity model has been used to design absorbers within 3-9 GHz [26], there is room for improvement in its accuracy. A simple fitting model was established in [21], and was applied to design wideband absorption within 2-12 GHz [27]. But it is only accurate for resistance surfaces between two dielectrics. Another study has introduced an effective permittivity model that considers the presence of air gaps between the resistive surface and dielectric, enabling the design of absorbers with a wide operating bandwidth of 1 to 10 GHz [28]. However, an effective permittivity for RSs printed on stratified dielectrics with metallic plate is rarely considered in the design of wideband absorber. Additionally, the absorption bandwidth of the absorbers can be extended to both low and high frequencies.

In this paper, a general effective permittivity for single- or multi-layer RSs printed on stratified dielectrics under considering metallic plate is established and used to design ultra-wideband absorbers. In the proposed methodology, the closed-form expressions between absorber parameters and values of resistors and capacitors are developed. The values of the lumped elements meeting a reflection goal can be obtained by a genetic algorithm (GA), which will be used to compute the absorber parameters by means of the expressions. The proposed method offers several advantages: 1) it develops a general effective permittivity for single- or multi-layer RSs printed on layered dielectrics; 2) it offers a fast method to design ultra-wideband absorbers; 3) the total thickness of the designed absorbers is very close to the Rozanov limit.

II. CAPACITIVE CIRCUIT MODEL AND EFFECTIVE PERMITTIVITY

The capacitive circuit is a convenient and effective method in the design of multilayer ultra-broadband absorbers. The capacitive circuit absorber can achieve impedance matching and good absorption performance within a broadband frequency region and overcome the limitations of grating lobes and harmonics of the fundamental resonance in the selected surface patterns at high frequencies [29], which provides a simple design and optimization process using GA.

A. Characteristics of Square Resistive Film Patch

For square resistive surface arrays, it can be considered as a series connection of a resistance and a capacitance [19]. The lumped resistance R is closely related to the sheet resistance Rs,

This work was supported in part by the Fundamental Research Funds for the Central Universities under Grant 2023-00178, the Postgraduate Research & Practice Innovation Program of Jiangsu Province under Grant 2023XSCX026, the Graduate Innovation Program of China University of Mining and Technology under Grant 2023WLKXJ094, and the National Natural Science Foundation of China under Grant 61771226 *(Corresponding author: L. Zhao).*

X. Kong, and L. Zhao are with the School of Information and Control Engineering, China University of Mining and Technology, Xuzhou, China (e-mail: xlkong@cumt.edu.cn, leizhao@cumt.edu.cn).

S. Zhang is with the Test Physics & Numerical Mathematical, National Key Laboratory of Science and Technology, Beijing, China (e-mail: zhangsj98@sina.com).

X. Pang and Y. Fu are with the High Performance Electromagnetic Window, Key Laboratory of Aeronautical Science and Technology, Jinan, China (e-mail: pangxiaoyu2004@126.com, fu1xiang@foxmail.com).

Z. Shen is with the School of Electrical and Electronic Engineering, Nanyang Technological University, Singapore. (e-mail: ezxshen@ntu.edu.sg).

Authorized licensed use limited to: CHINA UNIVERSITY OF MINING AND TECHNOLOGY. Downloaded on March 06,2024 at 11:53:19 UTC from IEEE Xplore. Restrictions apply.
© 2024 IEEE. Personal use is permitted, but republication/redistribution requires IEEE permission. See https://www.ieee.org/publications/rights/index.html for more information.

This article has been accepted for publication in IEEE Antennas and Wireless Propagation Letters. This is the author's version which has not been fully edited and content may change prior to final publication. Citation information: DOI 10.1109/LAWP.2024.3371930

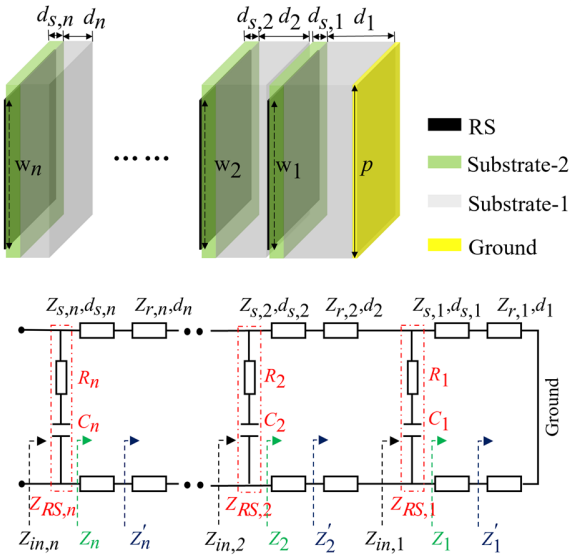

Fig.1. Multilayer absorber physical model and its equivalent circuit model.

the length of resistive surface and the period of unit cell, which can be evaluated by the following expression [22]:

$$R = R_s \frac{S}{A} = R_s \frac{p^2}{w^2} \tag{1}$$

where p is the period of the unit cell, w is the width of the square RS patch. S and A are the corresponding surface areas of the unit cell and RS, respectively. And dielectric losses of a substrate can be neglected when it is compared to RSs [19].

The equivalent capacitance C of the "embedded RS" can be calculated by the closed-form expression [23, 24]:

$$C = \varepsilon_{eff} C_0 = \varepsilon_{eff} \frac{2\varepsilon_0 p}{\pi} \left(\sin\left(\frac{\pi g}{2p}\right)\right)^{-1} \tag{2}$$

where $g=p-w$ is the gap between patches and $\varepsilon_0 = 8.854\times10^{-12}$ F/m is the permittivity of free-space. And C_0 represents the capacitance of RSs in free space. The effective permittivity ε_{eff} depends on the dielectric environment surrounding the RS.

B. Establishment of Equivalent Circuit Model

Absorbers with multilayer RSs can provide broadband absorption due to the dominance of ohmic losses in RSs. To obtain a wideband absorption, a thin substrate is selected for printing RSs and materials of low permittivity are selected as the interlayers. As shown in Fig.1, the physical structure of an absorber and its EC model of the multilayer absorber are established. Based on the transmission line theory, the substrate is considered to be an equal length transmission line, the metallic plate is considered as a short circuit, and the resistive surface patch is treated as a RC series circuit. The reflection coefficient related to the impedance of free-space (Z_0) and input impedance (Z_{in}) of the presented circuit model is [30]

$$\Gamma = \frac{Z_{in} - Z_0}{Z_{in} + Z_0} \tag{3}$$

The input impedance at i-layer (i =1, 2, … n) can be calculated by an iterative method as

$$Z_{RS,i} = R_i + \frac{1}{j\omega C_i} \tag{4}$$

$$Z_1' = jZ_{r,1} \tan(\beta_{r,1} d_1) \tag{5}$$

$$Z_i' = Z_{r,i} \frac{Z_{in,i-1}' + jZ_{r,i} \tan(\beta_{r,i} d_i)}{Z_{r,i} + jZ_{in,i-1}' \tan(\beta_{r,i} d_i)}, \quad i=2,3,\ldots n \tag{6}$$

$$Z_{in,i} = Z_i \| Z_{RS,i} = Z_{s,i} \frac{Z_i' + jZ_{s,i} \tan(\beta_{s,i} d_{s,i})}{Z_{s,i} + jZ_i' \tan(\beta_{s,i} d_{s,i})} \| Z_{RS,i} \tag{7}$$

where $Z_{s,i} = 377/\sqrt{\varepsilon_{s,i}}$ and $Z_{r,i} = 377/\sqrt{\varepsilon_{r,i}}$ are the characteristic impedances of substrate and interlayer with permittivity $\varepsilon_{s,i}$ and $\varepsilon_{r,i}$, respectively. $\beta_{s,i} = 2\pi\sqrt{\varepsilon_{s,i}}/\lambda$ and $\beta_{r,i} = 2\pi\sqrt{\varepsilon_{r,i}}/\lambda$ are the phase constant, $\omega = 2\pi f$. The lumped elements of R_i and C_i are the effective value of the square RS patch at i-layer.

The input impedance of the n-layer absorber can be obtained from Eq. (7) as

$$Z_{in} = Z_{in,n} = Z_{s,n} \frac{Z_n' + jZ_{s,n} \tan(\beta_{s,n} d_{s,n})}{Z_{s,n} + jZ_n' \tan(\beta_{s,n} d_{s,n})} \| Z_{RS,n} \tag{8}$$

C. Evaluation of Effective Permittivity

In this section, the general effective permittivity under considering metallic plate is derived to establish closed-form expressions between capacitors in the circuit model and absorber parameters. When the RS is embedded in two substrates with different thickness (d_1, d_2) and different permittivity (ε_1, ε_2), a simple conversion function for the average permittivity is [21]

$$\varepsilon_{av} = \varepsilon_{rd} + (1-\varepsilon_{rd}) e^{-\alpha(d/p)} \tag{9}$$

where $d = d_1 + d_2$ is the total thickness and p is the period of the unit cell. The ε_{rd} can be calculated by $\varepsilon_{rd} = (\varepsilon_1 d_1 + \varepsilon_2 d_2)/(d_1 + d_2)$. The shape-factor α is related to the geometry of RS, which obtained by the iterative Method of Momnets approach for different elements [21]. For a square RS patch array, the fitting value is α=13, while α=18 for the ring and cross patch array.

Numerous simulations under considering metal plate have shown that when the permittivity and thicknesses of the dielectric slabs on both sides of the RS are determined, i.e., ε_{av} is determined from Eq. (9), the thickness d_i and permittivity $\varepsilon_{r,i}$ dominate the effective permittivity. Here, the asymptotical method is employed to derived effective permittivity for RSs printed on layered dielectrics. To provide an insight into the general formula for the effective permittivity, the derivation procedure is as follows.

1) For $d_{s,i}/d_i \to 0$, the thickness of substrates for printing RSs is negligible compared to the interlayer. The effective permittivity can be written as

$$\varepsilon_{eff} = \frac{\varepsilon_{r,i} d_i + \varepsilon_{r,i+1} d_{i+1}}{d_i + d_{i+1}} + \left(1 - \frac{\varepsilon_{r,i} d_i + \varepsilon_{r,i+1} d_{i+1}}{d_i + d_{i+1}}\right) e^{-13\frac{d_i + d_{i+1}}{p}} \tag{10}$$

2) For $d_{s,i}/d_i \to \infty$, the thickness of the interlayer can be considered as zero compared to the substrate. The effective permittivity can be calculated as

$$\varepsilon_{eff} = \frac{\varepsilon_{s,i} d_{s,i} + \varepsilon_{s,i+1} d_{s,i+1}}{d_{s,i} + d_{s,i+1}} + \left(1 - \frac{\varepsilon_{s,i} d_{s,i} + \varepsilon_{s,i+1} d_{s,i+1}}{d_{s,i} + d_{s,i+1}}\right) e^{-13\frac{d_{s,i} + d_{s,i+1}}{p}} \tag{11}$$

3) For $\varepsilon_{r,i}$ =1, i.e., RS printed on substrate-air surface (the average permittivity $\varepsilon_{av,i} = (\varepsilon_{s,i}+1)/2$, the effective permittivity can be described as [28]

$$\varepsilon_{eff} = (\varepsilon_{av,i} - 1)(1 - 10^{-4\frac{d_{s,i}}{d_i}}) + 1 \tag{12}$$

4) To obtain sufficient data, numerous simulations with key parameters of d_{si}/d_i, $\varepsilon_{r,i}$, and $\varepsilon_{s,i}$ are performed. An expression for calculating the effective permittivity of RS at i-th layer is proposed by analogy to formula (12) and combining the two asymptotes as follows:

Authorized licensed use limited to: CHINA UNIVERSITY OF MINING AND TECHNOLOGY. Downloaded on March 06,2024 at 11:53:19 UTC from IEEE Xplore. Restrictions apply.
© 2024 IEEE. Personal use is permitted, but republication/redistribution requires IEEE permission. See https://www.ieee.org/publications/rights/index.html for more information.

This article has been accepted for publication in IEEE Antennas and Wireless Propagation Letters. This is the author's version which has not been fully edited and content may change prior to final publication. Citation information: DOI 10.1109/LAWP.2024.3371930

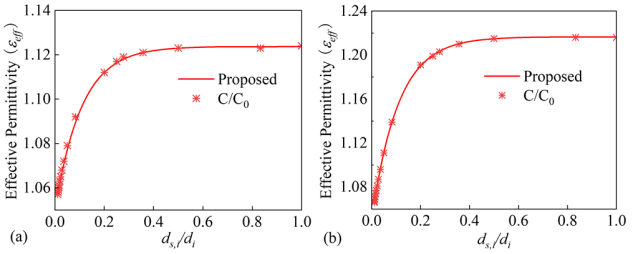

Fig.2. Effective permittivity computed by using C/C_0 and by using proposed fitting model. The following characteristics are used: (a) $\varepsilon_{s,i}$ =3, $d_{s,i}$=0.25, $\varepsilon_{r,i}$ = $\varepsilon_{r,i+1}$ =1.05, d_{i+1} =5, $d_{s,i}$/ d_i=(0:1). (b) $\varepsilon_{s,i}$ =3, $d_{s,i}$=0.25, $\varepsilon_{r,i}$ = $\varepsilon_{r,i+1}$ =1.05, d_{i+1} =1, $d_{s,i}$/ d_i=(0:1).

$$\varepsilon_{eff} = (\varepsilon_{av,i}-\varepsilon_{r,i})(1-10^{-4\frac{d_{s,i}}{d_i}})+\varepsilon_{r,i} \tag{13}$$

where the permittivity $\varepsilon_{av,i}$ (i =1, 2, … n-1)can be easily obtained from Eq. (9), i.e.,

$$\varepsilon_{av,i}=\varepsilon_{rd,i}+(1-\varepsilon_{rd,i})e^{-13(d_{s,i}+d_{i+1})/p} \tag{14}$$

$$\varepsilon_{rd,i}=\frac{\varepsilon_{s,i}d_{s,i}+\varepsilon_{r,i+1}d_{i+1}}{d_{s,i}+d_{i+1}} \tag{15}$$

and the nth-layer RSs printed at substrate-air interface, its average permittivity is [20]

$$\varepsilon_{av,n}=\frac{\varepsilon_{s,n}+1}{2} \tag{16}$$

Fig.2 illustrates the comparison between the proposed effective permittivity model, obtained through relation (13), and the numerically derived effective permittivity based on C/C_0, using simulation results [31]. The results show that the proposed model is consistent with the derived ones.

III. Design and Optimization of Absorbers

In multi-layered absorber design, EC and GA are combined to simplify impedance matching over a wide frequency range. The flow chart of the absorber design and optimization is shown in Fig. 3. In this method, absorber parameters of $d_{s,i}$, d_i, p, w_i and $R_{s,i}$ are treated as variables to find an optimal value satisfying the desired reflection characteristics. Then, the physical structure parameters of the absorbers with desired absorption performance can be derived by the closed-form expressions. Finally, the optimized structural parameters are validated by full-wave simulations.

A fitness function is given to evaluate how far the current iteration from the target.

$$Fitness = \sum_{i=1}^{m} W_i \times \sum_{j=1}^{N_i} \frac{|e_i(f_j)|^2}{N_i} \tag{17}$$

where i represents the i-th optimization goal, W_i is the weight factor, N_i and f_j refer to the number of frequencies and the j-th frequency in the i-th optimization goal. And $e_i(f_j)$ is the difference between the optimized response $R_i(f_j)$ and the target threshold $G_i(f_j)$, which can be described as:

$$e_i(f_j)=\begin{cases} R_i(f_j)-G_i(f_j) & if\ R_i(f_j)>G_i(f_j) \\ 0 & if\ R_i(f_j)\leq G_i(f_j) \end{cases} \tag{18}$$

When $R_i(f_j) \leqslant G_i(f_j)$, the difference $e_i(f_j)$ is equal to 0, which means it makes no contribution to the fitness function.

The relationship between the absorption bandwidth and number of layers can be obtained by summarizing the optimization data and design experience [9-18]. To simplify optimization process, $d_{s,i}$ and p are fixed to constants. In this

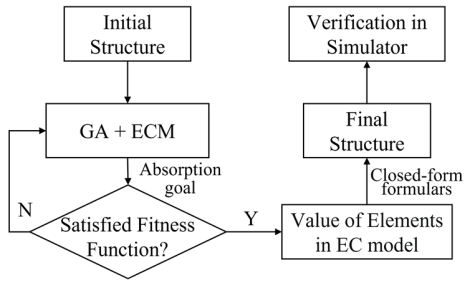

Fig.3. Flowchart of multilayer broadband absorber design and optimization utilizing proposed method.

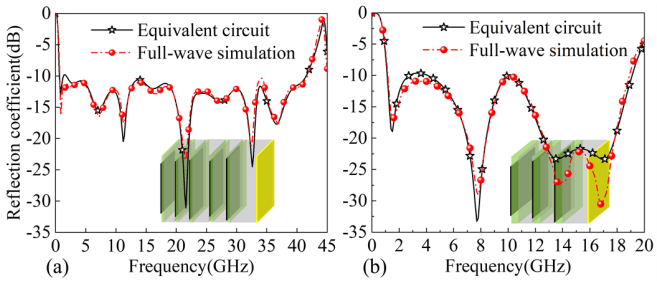

Fig.4. Comparison of reflection coefficient. (a) sample I. (b) sample II.

design, polyethylene terephthalate (PET) slabs ($\varepsilon_{s,i}$=3-j0.06) is selected as thin substrate and polymethacrylimide (PMI) foams ($\varepsilon_{r,i}$=1.05-j0.001) is selected as interlayer [32, 33]. Here, two prototypes are proposed to demonstrate the effectiveness of the proposed method. For Sample I, the reflection coefficient goal is set less than or equal to -10 dB within 0.6-40 GHz and $G_i(f_j)$ is equal to -10 dB in fitness function, and N_i is equal to 395. Its structural parameters are as follows: $R_{s,1}$=135 Ω/□, $R_{s,2}$=492 Ω/□, $R_{s,3}$=460 Ω/□, $R_{s,4}$=579 Ω/□, $R_{s,5}$=626 Ω/□, d_1=13 mm, d_2=13 mm, d_3=10 mm, d_4=6.5 mm, d_5=2.7 mm, w_1=41.7 mm, w_2=41 mm, w_3=36.6 mm, w_4=38.5 mm, w_5=27.3 mm, $d_{s,i}$=0.125 mm (i=1, 2… 5), and p=42 mm. For Sample II, the reflection coefficient goal of less than or equal to -10 dB and -20 dB within 1-12 GHz and 12-18 GHz respectively is configured and $G_i(f_j)$ is equal to -10 dB and -20 dB in fitness function, respectively. Moreover, N_i is equal to 171. Its parameters are as follows: $R_{s,1}$=215 Ω/□, $R_{s,2}$=416 Ω/□, $R_{s,3}$=437 Ω/□, d_1=14.8 mm, d_2=6.1 mm, d_3=5.3 mm, $d_{s,i}$=0.25 mm (i=1, 2, 3), w_1=23.5 mm, w_2=21.5 mm, w_3=17.4 mm, and p=24 mm. With the same optimized range of variable values, sample I and sample II took 68 s and 100 s using the proposed method, compared to 51 h and 6 h and 20 min using only GA, which run on computers of the same configuration with Intel(R) Core (TM) i5-10505 CPU @ 3.20GHz and 32GB RAM.

For validation of the proposed method, the optimized parameters are modeled and solved by using unit cell boundary condition in full-wave simulator to compare with the calculated results of the EC model. In Fig.4 (a), the reflection loss and working bandwidth for sample I are presented. The reflection loss from EC model and simulator are both less than -10 dB within 0.64-41.7 GHz (fractional bandwidth of 193.95%). Fig.4 (b) shows sample II and its reflection loss lower than -10 dB and -20 dB within 1.16-12.5 GHz and 12.5-18 GHz, respectively. Moreover, the reflection loss less than -10 dB operates from 1.16 GHz to 19.2 GHz, with a fractional bandwidth of 177.2%. The slight discrepancy between the

Authorized licensed use limited to: CHINA UNIVERSITY OF MINING AND TECHNOLOGY. Downloaded on March 06,2024 at 11:53:19 UTC from IEEE Xplore. Restrictions apply.
© 2024 IEEE. Personal use is permitted, but republication/redistribution requires IEEE permission. See https://www.ieee.org/publications/rights/index.html for more information.

This article has been accepted for publication in IEEE Antennas and Wireless Propagation Letters. This is the author's version which has not been fully edited and content may change prior to final publication. Citation information: DOI 10.1109/LAWP.2024.3371930

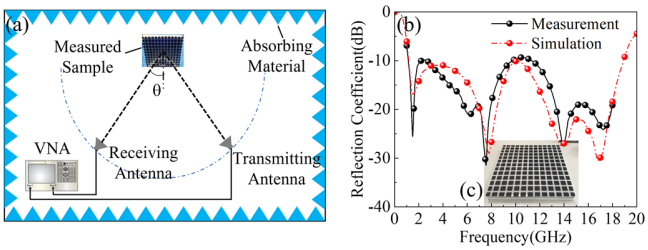

Fig.5. (a) Test equipment in a microwave anechoic chamber, (b) comparison of reflection parameters of EC model and full-wave simulation, (c) fabricated sample II.

optimized response and the goal response due to the fact that the two targets may be in conflict with each other and it is hard to make both targets reach the optimal value [34]. It is the best result obtained after several iterations of GA, so we confident it is an acceptable answer in wideband absorbers design.

According to Rozanov limit [35], the minimum thickness of nonmagnetic absorbers can be written as

$$d_{min}=\frac{\left|\int_0^\infty \ln|\rho(\lambda)|d\lambda\right|}{2\pi^2}\approx\frac{\left|\int_0^\infty |\Gamma(\lambda)|d\lambda\right|}{172} \tag{19}$$

where $\rho(\lambda)$ and $\Gamma(\lambda)$ are a function of wavelength of reflection coefficient in linear and dB version. The total thickness of sample I and II are 45.82 mm and 25.49 mm respectively, and their Rozanov limit thickness are 44.06 mm and 26.95 mm respectively.

The causality ratio can directly show the discrepancy between the design thickness and the theoretical thickness, which can be defined by [36]

$$R_c=\frac{d_t}{d_{min}} \tag{20}$$

where d_t is the total thickness of the designed absorbers. The causality ratio of sample I and sample II were obtained by calculation as 1.04 and 1.03, respectively.

IV. Experimental Verification

To further validate the accuracy of the proposed method, sample II is fabricated and measured. It consists of 13 × 13 units with a size of 312 mm ×312 mm, which is shown in Fig.5 (c). Each layer of RS is printed on PET substrate using screen printing technology. They are assembled with PMI foam and metal plates in the designed sequence to form the complete absorbers. In Fig.5 (a), two sets of broadband horn antennas (1–8 GHz; 2–18 GHz) are connected to the vector network analyzer (VNA) as transmitter and receiver in an anechoic chamber. The size of the former and later antenna is 240 mm×140 mm and 120 mm×80 mm, respectively. To satisfy the far-field condition, the two antennas are 2 m away from the sample II.

A metallic plate of the same size as the fabricated sample is used as reference to normalize the reflection parameters of the absorber sample. The measured reflection coefficient of the designed absorber under normal incidence is shown in Fig.5 (b). The measured and simulated results are in good agreement, which are less than -10 dB and -20 dB within 1.16-13 GHz and 13-18 GHz, respectively. Fig.6 shows the comparison between simulation and measurement of the absorber under transverse electric (TE) waves and transverse magnetic (TM) waves at different incident angles. It can be seen that the reflection loss

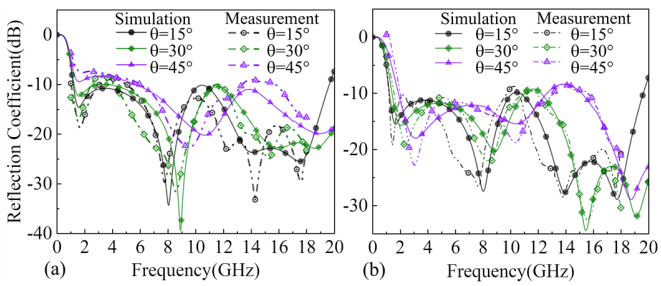

Fig.6. The comparison of simulated and measured results of the designed absorber under oblique incidence for (a) TE waves and (b) TM waves.

TABLE I
Comparation of Absorber Performance

Ref.	Reflection Loss(dB)	Operating Band(GHz)	Fractional Bandwidth	Thickness (mm)	Rc
[11]	-10	1-12.9	171.2%	26	1.09
[16]	-10	2.35-18	155%	17	1.23
[17]	-10	1-18	179%	30	1.17
[26]	-10	3-9	100%	10	1.48
[27]	-10	2-11.4	140.2%	14.35	1.15
[28]	-10	1.07-9.7	160.3%	25.27	1.07
This work	-10 -20	1.16-12.5 12.5-19.2	177.2%	26.95	1.03

Fractional Bandwidth (FBW) is defined by FBW=$(2\times(f_{max}-f_{min})/(f_{max}+f_{min}))\times100\%$, where f_{max}, f_{min} represents the lowest and highest frequency within absorption bandwidth.
The operating band, thickness and Rc are evaluated from published results

and operation bandwidth are relatively stable under oblique incidence up to 45°. Besides, the measured results are consistent with the simulation ones and the slight deviation may come from the sample manufacturing.

Table I shows the comparison of several recent designs in terms of operating band (fraction bandwidth), total thickness, causality ratio, etc. Meanwhile, the designed absorbers present many advantages, such as wide working frequency, small relative thickness and small causality ratio.

V. Conclusion

In this paper, an efficient method has been proposed to facilitate the design of ultra-wideband absorbers with multilayered RS patches. A general effective permittivity model is established to obtain the closed-form formulas between lumped elements in equivalent circuit and the parameters of the resistive surface. The utilization of equivalent circuit and genetic algorithms enables optimal values of the lumped elements to calculate the parameters of an absorber with a targeted specification. Two ultra-wideband absorbers (fractional bandwidth of 193.95% and 177.2%) have been optimized and designed to verify the validity and accuracy of the proposed method. Simulated and measured results have confirmed that the proposed method has the ability for fast design of wideband absorbers with targeted absorption characteristics.

Authorized licensed use limited to: CHINA UNIVERSITY OF MINING AND TECHNOLOGY. Downloaded on March 06,2024 at 11:53:19 UTC from IEEE Xplore. Restrictions apply.
© 2024 IEEE. Personal use is permitted, but republication/redistribution requires IEEE permission. See https://www.ieee.org/publications/rights/index.html for more information.

This article has been accepted for publication in IEEE Antennas and Wireless Propagation Letters. This is the author's version which has not been fully edited and content may change prior to final publication. Citation information: DOI 10.1109/LAWP.2024.3371930

REFERENCES

[1] H. Jiang, W. Yang, S. Lei, B. Chen, H. Hu and Z. Zhao, "A conformal metamaterial-based optically transparent microwave absorber with high angular stability," *IEEE Antennas Wireless Propag. Lett.*, vol. 20, no. 8, pp. 1399-1403, Aug. 2021.

[2] B. Araújo, G. Siqueira, E. Kemptner, M. Weber, C. Junqueira and M. Mosso, "An ultrathin and ultrawideband metamaterial absorber and an equivalent circuit parameter retrieval method," *IEEE Trans. Antennas Propag.*, vol. 68, no. 5, pp. 3739-3746, May. 2020.

[3] Y. Huang, J. Luo, M. Pu, Y. Guo, Z. Zhao, X. Ma, X. Li and X. Luo, "Catenary electromagnetics for ultra-broadband lightweight absorbers and large-scale flat antennas," *Adv. Sci.*, vol. 6, no. 7, p. 1801691, Apr. 2019.

[4] H. Sheokand, G. Singh, S. Ghosh, J. Ramkumar, S. A. Ramakrishna and K. V. Srivastava, "An optically transparent broadband microwave absorber using interdigital capacitance," *IEEE Antennas Wireless Propag. Lett.*, vol. 18, no. 1, pp. 113-117, Jan. 2019.

[5] M. M. Tirkey and N. Gupta, "Broadband polarization-insensitive inkjet-printed conformal metamaterial absorber," *IEEE Trans. Electrmagn. Compat.*, vol. 63, no. 6, pp. 1829-1836, Dec. 2021.

[6] M. Li, S. Q. Xiao, Y. Y. Bai, and B. Z. Wang, "An ultrathin and broadband radar absorber using resistive FSS," *IEEE Antennas Wireless Propag. Lett.*, vol. 11, pp. 748-751, Jul. 2012.

[7] J. Chen, Z. Hu, G. Wang, X. Huang, S. Wang, X. Hu and M. Liu, "High-impedance surface-based broadband absorbers with interference theory," *IEEE Trans. Antennas Propag.*, vol. 63, no. 10, pp. 4367-4374, Oct. 2015.

[8] P. Chen, X. Kong, J. Han, W. Wang, K. Han, H. Ma, L. Zhao and X. Shen, "Wide-angle ultra-broadband metamaterial absorber with polarization insensitive characteristics," *Chinese Phys. Lett.*, vol. 38, no. 2, p. 27801, Jan. 2021.

[9] W. Yu, G. Q. Luo, Y. Yu, W. Cao, Y. Pan and Z. Shen, "Dual-polarized band absorptive frequency selective rasorber using meander-line and lumped resistors," *IEEE Trans. Antennas Propag.*, vol. 67, no. 2, pp. 1318-1322, Feb. 2019.

[10] Y. Shang, Z. Shen, and S. Xiao, "On the design of single-layer circuit analog absorber using double-square-loop array," *IEEE Trans. Antennas Propag.*, vol. 61, no. 12, pp. 6022-6029, Dec. 2013.

[11] Z. Yao, S. Xiao, Y. Li, and B. Wang, "On the design of wideband absorber based on multilayer and multi resonant FSS array," *IEEE Antennas Wireless Propag. Lett.*, vol. 20, no. 3, pp. 284-288, Mar. 2021.

[12] B. Zhang, C. Jin, and Z. Shen, "Low-profile broadband absorber based on multimode resistor-embedded metallic strips," *IEEE Trans. Microw. Theory Techn.*, vol. 68, no. 3, pp. 835-843, Mar. 2020.

[13] W. Pan, X. Yu, J. Zhang, and W. Zeng, "A broadband Terahertz metamaterial absorber based on two circular split rings," *IEEE J. Quantum Elect.*, vol. 53, no. 1, pp. 1-6, Feb. 2017.

[14] B. F. Al-Azzawi, J. M. Rigelsford, and R. J. Langley, "A systematic transmission line model for the analysis of self-resonant structures within multi-layer dielectric media," *IEEE Trans. Microw. Theory Techn.*, vol. 67, no. 10, pp. 4118-4129, Oct. 2019.

[15] X. Kong, H. Ma, P. Chen, C. Liang, and W. Wang, "Design of ultra-wideband metamaterial absorber based on resistance films," *Chinese Journal of Radio Science*, vol. 36, no. 06, pp. 947-952, 2021.

[16] M. Li, B. Muneer, Z. Yi, and Q. Zhu, "A broadband compatible multispectral metamaterial absorber for visible, near-infrared, and microwave bands," *Adv. Opt. Mater.*, vol. 6, no. 9, p. 1701238, May. 2018.

[17] Z. Du, J. Liang, T. Cai, X. Wang, Q. Zhang, T. Deng, B. Wu, R. Mao and D. Wang, "Ultra-light planar meta-absorber with wideband and full-polarization properties," *Opt. Express*, vol. 29, no. 5, p. 6434, Mar. 2021.

[18] C. Liang, X. Kong, F. Wang, R. Xu Y. Fu, X. Pang, S. Zhang, X. Shen, L. Zhao, "A broadband perfect metamaterial absorber with angle-insensitive characteristics," *J. Electromagn. Wave Appl.*, vol. 37, no. 3, pp. 401-410, Mar. 2023.

[19] F. Costa, S. Genovesi, A. Monorchio, and G. Manara, "A circuit-based model for the interpretation of perfect metamaterial absorbers," *IEEE Trans. Antennas Propag.*, vol. 61, no. 3, pp. 1201-1209, Mar. 2013.

[20] O. Luukkonen, C. Simovski, G. Granet, G. Goussetis, D. Lioubtchenko. A. V. Raisanen, and S. A. Tretyakov, "Simple and accurate analytical model of planar grids and high-impedance surfaces comprising metal strips or patches," *IEEE Trans. Antennas Propag.*, vol. 56, no. 6, pp. 1624-1632, Jun. 2008.

[21] F. Costa, A. Monorchio, and G. Manara, "Efficient analysis of frequency-selective surfaces by a simple equivalent-circuit model," *IEEE Antenn. Propag. Mag.*, vol. 54, no. 4, pp. 35-48, Aug. 2012.

[22] F. Costa, A. Monorchio, and G. Manara, "Analysis and design of ultra-thin electromagnetic absorbers comprising resistively loaded high impedance surfaces," *IEEE Trans. Antennas Propag.*, vol. 58, no. 5, pp. 1551-1558, May. 2010.

[23] F. Costa and A. Monorchio, "Closed-form analysis of reflection losses in microstrip reflectarray antennas," *IEEE Trans. Antennas Propag.*, vol. 60, no. 10, pp. 4650-4660, Oct. 2012.

[24] S. A. Tretyakov and C. R. Simovski, "Dynamic model of artificial reactive impedance surfaces," *J. of Electromagn. Waves and Appl.*, vol. 17, no. 1, pp. 131-145, Dec. 2003.

[25] K. W. Whites and R. Mittra, "An equivalent boundary condition model for lossy planar periodic structures at low frequencies," *IEEE Trans. Antennas Propag.*, vol. 44, no. 12, pp. 1617-1629, Dec. 1996.

[26] Y. Han, W. Che, C. Christopoulos, Y. Xiong, and Y. Chang, "A fast and efficient design method for circuit analog absorbers consisting of resistive square-loop arrays," *IEEE Trans. Electrmagn. Compat.*, vol. 58, no. 3, pp. 747-757, Jan. 2016.

[27] H. Li, H. Dong, Y. Zhang, N. Mou, Y. Xin, R. Deng and L. Zhang, "Transparent ultra-wideband double-resonance-layer metamaterial absorber designed by a semiempirical optimization method," *Opt. Express*, vol. 29, no. 12, p. 18446, Jun. 2021.

[28] M. I. Hossain, N. Nguyen-Trong, K. H. Sayidmarie, and A. M. Abbosh, "Equivalent circuit design method for wideband nonmagnetic absorbers at low microwave frequencies," *IEEE Trans. Antennas Propag.*, vol. 68, no. 12, pp. 8215-8220, Dec. 2020.

[29] A. K. Zadeh and A. Karlsson, "Capacitive circuit method for fast and efficient design of wideband radar absorbers," *IEEE Trans. Antennas Propag.*, vol. 57, no. 8, pp. 2307-2314, Aug. 2009.

[30] D. M. Pozar, *Microwave Engineering*, 4th ed. Hoboken, NJ, USA: John Wiley & Sons, 2005, pp. 28-30.

[31] F. Costa, "A simple effective permittivity model for metasurfaces within multilayer stratified media," *IEEE Trans. Antennas Propag*., vol. 69, no. 8, pp. 5148-5153, Aug. 2021.

[32] C. Zhang, S. Yin, C. Long, B. Dong, D. He, and Q. Cheng, "Hybrid metamaterial absorber for ultra-low and dual-broadband absorption," *Opt. Express*, vol. 29, no. 9, pp. 14078, Apr. 2021.

[33] T. Liu and S. Kim, "Design of ultra-wide bandwidth double-layer electromagnetic wave absorbers with square-loop frequency selective surfaces," *Microw. Opt. Technol. Lett.*, vol. 60, no. 8, pp. 2013-2018, Jun. 2018.

[34] M. Zhou and S. Sun, *Genetic algorithms: theory and application*. Beijing, China: National Defense Industry Press, 1999, pp.130-134.

[35] K. N. Rozanov, "Ultimate thickness to bandwidth ratio of radar absorbers," *IEEE Trans. Antennas Propag.*, vol. 48, no. 8, pp. 1230-1234, Aug. 2000.

[36] S. Qu, Y. Hou, and P. Sheng, "Conceptual-based design of an ultrabroadband microwave metamaterial absorber," *Proc. Natl. Acad. Sci. U.S.A.*, vol. 118, no. 36, Aug. 2021.

Authorized licensed use limited to: CHINA UNIVERSITY OF MINING AND TECHNOLOGY. Downloaded on March 06,2024 at 11:53:19 UTC from IEEE Xplore. Restrictions apply.
© 2024 IEEE. Personal use is permitted, but republication/redistribution requires IEEE permission. See https://www.ieee.org/publications/rights/index.html for more information.